Implementation algorithm of a generalised plasticity model for swelling clays

M. Sánchez [a,*], A. Gens [b], L. Guimarães [c], S. Olivella [b]

[a] Department of Civil Engineering, University of Strathclyde, Glasgow, UK
[b] Department of Geotechnical Engineering and Geosciences, Universitat Politècnica de Catalunya, (UPC), Barcelona, Spain
[c] Department of Civil Engineering, Universidade Federal de Pernambuco, Recife, Brazil

ARTICLE INFO

ABSTRACT

A multi-mechanism generalisation of Sloan's integration scheme for elasto-plastic laws has been developed in order to implement a double structure model for expansive clays into a FE code. The constitutive model is built on a conceptual approach for unsaturated expansive soils in which the fundamental characteristic is the explicit consideration of the two pore levels often present in expansive clays. The distinction between macro and microstructure provides the opportunity to take into account the dominant phenomena that affect the behaviour of each structural level and the main interactions between them. The model is formulated using concepts of classical and generalised plasticity theories. The integration scheme proposed can deal with the two plastic mechanisms defined in the model and can incorporate the effects of strains, suction and temperature in the stress integration process. A large scale heating test is analysed to check the capabilities of the implemented model to simulate an actual problem involving complex thermo-hydro-mechanical stress paths. The performance of the model has been very satisfactory and the proposed integration scheme has proved to be robust and efficient in solving a highly non-linear coupled problem.

© 2008 Elsevier Ltd. All rights reserved.

1. Introduction

The study of expansive soils has been the subject of increasing interest in the last few years. A major aspect is the possible use of those materials as engineered barriers in radioactive waste repositories. Significant THM (thermo-hydro-mechanical) phenomena take place in the clay barrier and its near field due to the combined actions of heating arising from the canister, and hydration from the surrounding rock. However, the interest in these materials is not limited to nuclear waste disposal applications, but they are present in other engineering problems such as shallow and deep foundations, slopes with stability problems, or desiccation and formation of cracks in soils in arid regions.

Numerical models are useful tools for the design and assessment of geotechnical problems in general and they emerge as indispensable when the interest is focused on performance assessment involving long-term predictions. A typical example is the design of a repository for high level radioactive waste in which it is necessary to predict its THM behaviour over periods lasting thousands of years. Constitutive models able to reproduce correctly clay behaviour under the complex THM paths envisaged for the clay barrier are a basic component of that kind of analysis. The clay fabric plays a fundamental role to understand and to reproduce correctly the behaviour of expansive clays as revealed in a number of recent studies [3–7]. Gens and Alonso [3] proposed a general approach to analyze the behaviour of expansive clays in which the fundamental characteristic is the explicit consideration of the two dominant structure levels often present in swelling clays. Elasto-plastic models based on that double structure approach have been widely used as a conceptual framework to describe the behaviour of swelling materials and also to perform analyses at point integration level (i.e. [4–7]). However, their inclusion and exploitation in a finite element program to solve actual boundary value problems has not been done previously.

A refined Euler scheme with automatic sub-stepping and errors control based on Sloan's scheme [1,2] is proposed in this paper in order to implement the double structure model presented in Sánchez et al. [7] in the finite element program CODE_BRIGHT [8]. A feature of the double structure model is that the soil behaviour can be regarded as the result of the joint action of several mechanisms that can act simultaneously. Therefore, the proposed scheme is a multi-mechanism generalisation of Sloan's one [1,2] for the particular conditions of the double structure model. A great advantage of Sloan's scheme is that it has been widely tested in a number of geotechnical problems proving its accuracy, robustness and efficiency.

* Corresponding author. Tel.: +44 141 548 3273; fax: +44 141 553 2066.
E-mail address: marcelo.sanchez@strath.ac.uk (M. Sánchez).

The paper is organized as follows: firstly the main components of the model are outlined; secondly, the scheme proposed to implement the constitutive model in the finite element code is described; thirdly, an application case that shows the capabilities of the model is presented; finally, the main conclusions of the work are given.

2. Model formulation

Soil fabric plays a crucial role to understand and reproduce the behaviour of expansive clays. The pore size distribution of swelling clays often exhibits two dominant pore sizes. For example Fig. 1 shows the results of mercury intrusion porosimetry tests of statically compacted samples of FEBEX bentonite for two specimens compacted to different values of dry density (ρ_d) [6]. The pore size distribution is clearly bi-modal and the two dominant pores size may be associated with two basic structural levels (Fig. 1): (i) the macrostructure, related to the global arrangements of clay aggregates (i.e. the skeleton of the material), enclosing macropores between them; (ii) the microstructure, which corresponds to the active clay minerals and their vicinity, present inside the aggregates.

In this type of soils there are plastic mechanisms in addition to those observed in non-swelling materials. Those additional mechanisms can be attributed to the interaction between the macrostructure and the microstructure [3]. This kind of irreversible behaviour generally appears at any value of applied suction and it is difficult to determine the initiation of the yielding [7]. Those facts encourage the use of the generalised plasticity theory to describe these plastic mechanisms [7]. In a generalised plasticity model the yield function is not defined or it is not defined in an explicit way [9]. The advantages in using the generalised plasticity theory to model the plastic mechanisms ascribed to the interaction between structures are presented in detail in [7].

The model is defined in terms of the three stress invariants ($p, J, \ominus$) suction (s) and temperature (T). The stress invariants are defined in the Appendix A. To formulate the double structure model is necessary to define laws for: (i) the macrostructural level, (ii) the microstructural level and (iii) the interaction between both structural levels. The full mathematical framework is presented in Sanchez et al. [7], herein only the main components of the model are briefly introduced for the sake of completeness. Additional information of the model is presented in the Appendix A. Table 1 presents the notation and nomenclature adopted in this work.
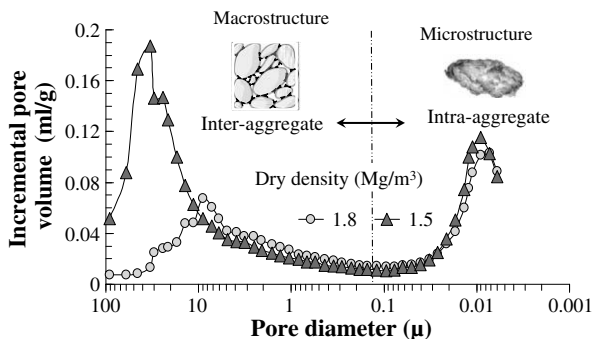

Fig. 1. Distributions of incremental pore volume for two statically compacted samples of FEBEX bentonite [6].

2.1. Macrostructural model

The inclusion of this structural level in the analysis allows the consideration of phenomena that affect the skeleton of the material, for instance deformations due to loading and/or collapse of the macrostructure. The BBM (Barcelona Basic Model) has been adopted to describe the macrostructural behaviour [12]. The BBM considers two stress variables to model the unsaturated behaviour: the net stress ($\boldsymbol{\sigma}$) computed as the excess of the total stresses over the gas pressure, and the matric suction (s), computed as the difference between gas pressure and liquid pressure ($p_g - p_l$). Fig. 2a shows the BBM yield surface (F_{LC}), which is defined as follows:

$$F_{LC} = 3J^2 - \left[\frac{g(\theta)}{g(-30°)}\right]^2 M^2 (p + p_s)(p_0 - p) = 0 \tag{1}$$

where M is the slope of the critical state, p_0 is the apparent unsaturated isotropic pre-consolidation pressure at a specific value of suction, and p_s considers the dependence of shear strength on suction and temperature. To complete the definition of the yield surface as set out in (1), it is possible, in principle, to adopt any suitable Lode's angle function, $g(\theta)$. For instance, in the CODE_BRIGHT code used in the analysis reported in this paper, the following functions are available: Von Mises (i.e. $g(\theta = $ constant), Mohr–Coulomb and Van Eekelen [13]. Other functions could be considered such as the one suggested in [10], which applies to soils with a friction angle less than 22° (to ensure a convex yield surface in the deviatoric plane) or the one recommended in [11], which applies to a friction angle up to 48.6°.

The trace of the yield function on the isotropic p–s plane is called LC (loading–collapse) yield curve because it represents the locus of activation of irreversible deformations due to loading increments or to collapse. The position of the LC curve is given by the pre-consolidation yield stress of the saturated state, p_0^* (hardening variable) that varies with plastic volumetric strain according to the following hardening law:

$$\dot{p}_0^* = p_0^* \frac{(1+e)}{(\lambda_{(0)} - \kappa)} \dot{\varepsilon}_v^p \tag{2}$$

where e is the void ratio, $\dot{\varepsilon}_v^p$ is the volumetric plastic strain, κ is the elastic compression index for changes in p and $\lambda_{(0)}$ is the stiffness parameter for changes in p for virgin states of the soil in saturated condition. In addition, the model is able to describe the reduction of the size of the yield surface and the strength of the material with the increase of temperature, according to the model proposed in Gens [14].

2.2. Microstructural model

The microstructure is the seat of the basic physico-chemical phenomena occurring at clay particle level. The strains arising from microstructural phenomena are considered nonlinear elastic and volumetric [3]. The microstructural strains are proportional to the microstructural effective stress ($\hat{p}$) through a microstructural bulk modulus according to

$$\hat{p} = p + \chi s \quad \text{(a)}; \quad \dot{\boldsymbol{\varepsilon}}_{vm} = \frac{\dot{\hat{p}}}{K_m} = \frac{\dot{p}}{K_m} + \chi \frac{\dot{s}}{K_m} \quad \text{(b)} \tag{3}$$

where the subscript m refers to the microstructural level, the subscript v refers to the volumetric component of the strains, K_m is the microstructural bulk modulus and χ is a parameter normally dependent on the degree of saturation of the microstructure. The parameter χ is included only to account for the possibility that the microstructure may become unsaturated. However, generally a constant value of $\chi = 1$ is adopted, since the micro-structural level, associated with the behaviour of expansive clay particles, is very

Table 1
Notation

$\boldsymbol{\alpha}_s$	elastic vector associated with suction	e_M	macrostructural level void ratio
$\boldsymbol{\alpha}_T$	elastic vector associated with temperature	e_m	microstructural level void ratio
α	parameter related to the plastic potential	F_{LC}	BBM yield surface
α_0	parameter for elastic thermal strain	F_{NL}	Neutral Line
α_1	parameter that relates p_o^* with T	fs,c	interaction function (s: swelling, c: compression)
α_2	parameter for elastic thermal strain	G	plastic potential
α_3	parameter that relates p_o^* with T	G_t	shear modulus
α_m	parameter controlling the microstructural soil stiffness	g	a lode angle function
$\boldsymbol{\beta}_s$	elasto-plastic vector associated with suction	$\mathbf{H}$	hardening modulus matrix
β_m	parameter controlling the microstructural soil stiffness	$\mathbf{H}^c$	critical softening matrix.
χ	F_{NL}slope	$\overline{\mathbf{H}}$	effective hardening matrix
ΔT	temperature increment $(T-T_0)$	$\mathbf{I}$	identity matrix
$\boldsymbol{\varepsilon}$	strain vector. $\left\{\varepsilon_x, \varepsilon_y, \varepsilon_z, \gamma_{xy}, \gamma_{xz}, \gamma_{yz}\right\}^T$	J	2nd stress invariant of deviatoric stress tensor
$\dot{\boldsymbol{\varepsilon}}^e$	elastic strain increment due to stress changes	K	global bulk modulus
$\dot{\boldsymbol{\varepsilon}}_s^e$	elastic strain increment due to suction changes	K_s	macrostructural bulk modulus for changes in suction
$\dot{\boldsymbol{\varepsilon}}_T^e$	elastic strain increment due to temperature changes	K_T	macrostructural bulk modulus for changes in temperature
ε_{vm}	elastic volumetric strain at microstructural level	K_M	macrostructural bulk modulus for changes in mean stress
ε_v^p	total plastic volumetric strain	K_m	microstructural bulk modulus for changes in mean stress plus suction
ε_{vi}^p	plastic volumetric strain related to i plastic mechanism $(i = lc, \beta)$	k	parameter describing the increase in cohesion with suction
$\boldsymbol{\gamma}_s$	elasto-plastic vector associated with suction	LC	Loading–collapse yield surface (BBM)
$\boldsymbol{\gamma}_T$	elasto-plastic vector associated with temperature	$\mathbf{m}$	auxiliary unit vector $\mathbf{m}^T = (1,1,1,0,0,0)$
η	stress ratio	$\mathbf{m}_{LC}$	flow rule direction of BBM
κ	macrostructural elastic stiffness parameter for changes in mean stress	$\mathbf{m}_\beta$	flow rule direction of mechanism β
κ_s	macrostructural elastic stiffness parameter for changes in suction	M	slope of critical state line
κ_m	parameter controlling the microstructural soil stiffness	MC	microstructural contraction path
$\lambda_{(s)}$	macrostructural compressibility parameter for changes in net mean stress for virgin states of soil at suction s	MS	microstructural swelling path
θ	Lode's angle	$\hat{p}$	microstructural effective stress
ρ	parameter that relates cohesion and T	p	mean net stress
$\boldsymbol{\sigma}_t$	total stress vector. $\left\{\sigma_x, \sigma_y, \sigma_z, \tau_{xy}, \tau_{xz}, \tau_{yz}\right\}^T$	p_c	reference stress
$\boldsymbol{\sigma}$	net stress vector $(\boldsymbol{\sigma}_t - \mathbf{I}\, p_g)$	p_0	net mean yield stress at current suction and temperature
$\hat{\boldsymbol{\sigma}}$	generalised stress vector	p_0^*	net mean yield stress for saturated conditions at reference temperature
ζ	parameter controlling the rate of increase of macrostructural soils stiffness with suction	p_{0T}^*	net mean yield stress for saturated conditions at current temperature
$\mathbf{D}_e$	elastic matrix	r	parameter defining the minimum macrostructural soil compressibility
$\mathbf{D}_{ep}$	elasto-plastic matrix	s	matric suction: difference between gas pressure and liquid pressure $(p_g - p_l)$
e	void ratio	T	temperature $(T_0 =$ reference temperature)

likely to be saturated [3]. In very active expansive clays this assumption can be supported by the high affinity of the active clay minerals by water, which maintain the interlayer space and micropores saturated even at relatively high suction. Under this condition mean effective stress control the mechanical behaviour at microstructural level [3]. Hydraulic equilibrium is assumed between the water potentials of both structural levels, the extension to non equilibrium conditions is presented in [5,15].

The concept of a neutral line (NL) is introduced corresponding to constant $\hat{p}$ and no microstructural deformation (Fig. 2b). The NL divides the p–s plane into two parts, defining two main generalized stress paths, which are identified as MC (microstructural contraction) when there is an increase in $\hat{p}$ and MS (microstructural swelling) in the opposite case.

2.3. Interaction between macro and micro structure

Based on experimental evidence, it is assumed that the macrostructure is affected by microstructural deformations generally in an irreversible way [3]. A hypothesis of the model is that the plastic deformations of the macrostructure (ε_{vM}^p) induced by microstructural effects are proportional to the microstructural strains (ε_{vm}) according to interaction functions f [7]. The total plastic macrostructural strains (i.e. the sum of the plastic strains induced by the yielding of the macrostructure, ε_{LC}^p, plus that induced by the microstructure, $\varepsilon_{vM \to m}^p$) are evaluated using (4):

$$\dot{\boldsymbol{\varepsilon}}_{vM}^p = \dot{\boldsymbol{\varepsilon}}_{vLC}^p + \boldsymbol{\varepsilon}_{vM \to m}^p = \dot{\boldsymbol{\varepsilon}}_{vLC}^p + f\dot{\boldsymbol{\varepsilon}}_{vm} \qquad (4)$$

Two interaction functions f are defined: f_c for MC paths and f_S for MS paths. The interaction functions depend on the ratio p/p_0 [7]. Examples of interaction functions are shown in Section 5 (Fig. 6). The ratio p/p_0 is a measure of the degree of openness of the macrostructure relative to the applied stress state [3]. When this ratio is low, it implies a dense packing of the material and it is expected that, under this condition (dense macrostructure), the microstructural swelling (MS path) affects strongly the global arrangements of clay aggregates, inducing large macrostructural plastic strains. In this case the microstructure effects induce a more open macrostructure, which implies a macrostructural softening. On the other hand, when the microstructure contracts (MC path) the induced macrostructural plastic strains are larger with open macrostructures, that is, for values of p/p_0 close to 1. Under this path the clay tends to a more dense state, which implies a hardening of the macrostructure. The result of the coupling between macro and micro levels is reflected in the value of p_0^*, the hardening variable of the macrostructure (Fig. 2a), which depends, through (2), on the total plastic volumetric strain (4). In this way the effect of microstructural processes on the global arrangements of aggregates is taken into account [7].

To describe correctly the soil behaviour, the definition of specific elasto-plastic laws for each domain is required according to the microstructural stress path followed (MC or MS). Generalised plasticity theory can deal with such conditions, allowing the consideration of two directions of different behaviour and the formulation of proper elasto-plastic laws for each region. Thus, a complete description of a generalised model includes the definition of the: (i) loading and unloading direction, (ii) plastic flow direction, and (iii) a plastic modulus [7].

Equivalent to loading/unloading directions in conventional stress/strain formulations, two vectors may be defined at every point of the stress space. One vector indicates the MC direction and the other the MS direction. Given a generalised stress state and stress increment, the criterion to identify the microstructural stress path is specified as (Fig. 2b):
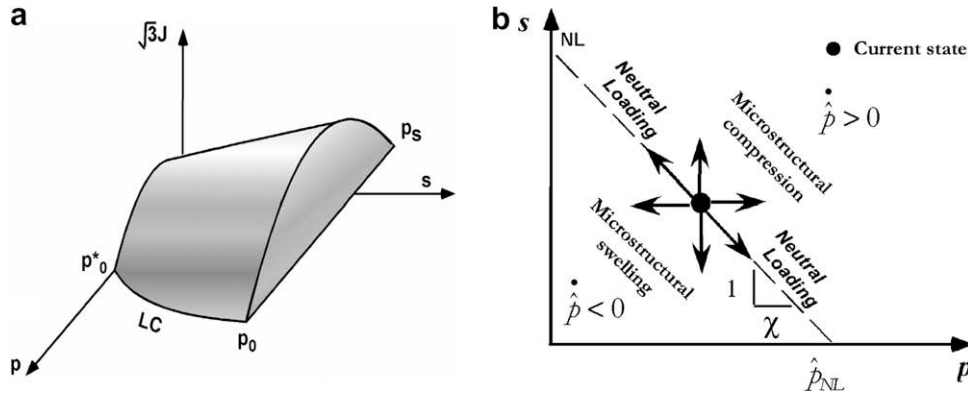
Fig. 2. (a) BBM yield surface. (b) Microstructural load directions on the p–s plane.

Microstructural compression criterion : $\hat{\mathbf{n}}_C^T \cdot \dot{\hat{\boldsymbol{\sigma}}}^e > 0$ (MC path) (5)

Microstructural swelling criterion : $\hat{\mathbf{n}}_S^T \cdot \dot{\hat{\boldsymbol{\sigma}}}^e > 0$ (MS path) (6)

Neutral loading : $\hat{\mathbf{n}}_\beta^T \cdot \dot{\hat{\boldsymbol{\sigma}}}^e = 0$ (NL path) (7)

where $\dot{\hat{\boldsymbol{\sigma}}}^e$ is the elastic generalised stress increment, $\hat{\mathbf{n}}_C^T$ and $\hat{\mathbf{n}}_S^T$ are the microstructural compression and swelling directions. In [7] the other model ingredients are introduced in detail.

3. Elasto-plastic stress–strain relations

Consequently, the constitutive model described contains two plastic mechanisms:

- A plastic mechanism associated with the yield of the macrostructure defined by a classical plasticity law.
- A plastic mechanism associated with the interaction between microstructure and macrostructure described by a generalised plasticity approach.

In classical plasticity theory, it is assumed that the material behaves either as an elastic or an elasto-plastic solid. The yield surface defines the transition from elasticity to plasticity, stress states inside the yield surface are considered as elastic ($F < 0$). In generalised plasticity theory, the state of the material is determined directly from the control variables: generalised stresses, strains and a finite number of internal variables. A process of loading is defined as elastic if the set of internal variables remains unchanged.

In the case of a purely (nonlinear) elastic loading, the stress increment is related to the increment of strains, suction and temperature by the following relationship:

$$\dot{\boldsymbol{\sigma}} = \mathbf{D}_e \cdot \dot{\boldsymbol{\varepsilon}}^e + \alpha_s \dot{s} + \alpha_T \dot{T} \tag{8}$$

where $\mathbf{D}_e$ is the global elastic matrix that considers the elastic component of both structural levels. $\boldsymbol{\alpha}_T$ and $\boldsymbol{\alpha}_s$ are the elastic vectors associated to temperature and suction respectively.

When a loading process is inelastic, the material behaviour is described by elasto-plastic mechanisms that can be activated during the loading process. A multidissipative approach [16] has been adopted to derive the general elasto-plastic relations [7] that can be expressed as follows:

$$\dot{\boldsymbol{\sigma}} = \mathbf{D}_{ep} \cdot \dot{\boldsymbol{\varepsilon}} + \gamma_s \dot{s} + \gamma_T \dot{T} \tag{9}$$

where $\boldsymbol{D}_{ep}$ is the global elasto-plastic matrix, γ_T, and γ_s are the elasto-plastic vectors associated with temperature and suction, respectively. The expressions for the vectors and matrices in (8) and (9) are presented in the Appendix A.

4. Model implementation

A refined explicit Euler method with automatic sub-stepping and errors control has been adopted to implement the model presented in the previous section in the finite element code CODE_BRIGHT. The proposed scheme is a generalisation of algorithm proposed in [1,2], considering the erratum published in [17]. CODE_BRIGHT is a tool designed to analyze numerically coupled THM problems in geological media that allows the performance of analysis in 1, 2 and 3 dimensions [8]. The advantages in using schemes based on explicit Euler method with error control to integrate highly no linear models have been discussed elsewhere [2,17–19]. As a summary it can be mentioned that: (i) it is possible to control the integration errors (based on a prescribed error tolerance); (ii) it is a robust and an efficient scheme even for highly non-linear models; (iii) only the first derivatives of the yield surface and plastic potential are required (reduction of CPU time); (iv) this type of scheme provides an open and flexible framework to incorporate additional irreversible mechanisms.

The proposed algorithm can deal with the two plastic mechanisms defined in the model and it can consider the effects of strains, suction and temperature in the stress integration process. Four different cases can be distinguished in relation to the current stress state and the number of irreversible mechanisms active:

- Case I: Behaviour purely (nonlinear) elastic.
- Case II. Only the plastic mechanism associated with the coupling with the two structural levels is active.
- Case III. Only the plastic mechanism associated with the yielding of the macrostructure is active.
- Case IV. The two plastic mechanisms are active simultaneously.

The control variables of the problem are strains, suction and temperature. Following a similar procedure to that proposed in [19], the suction and temperature are treated as additional strain components. For simplicity's sake, the generic name of generalised strains is assigned to this enlarged strain vector (i.e. including strain, suction and temperature). The initial state of the material is given by the initial stresses, the initial values of hardening parameters (p_0^* and $\hat{p}_{NL}$) and the initial values of the history variables (i.e. e_M and e_m, macro and micro void ratio respectively). Therefore four internal variables r are considered in these model (p_0^*, $\hat{p}_{NL}$, e_M and e_m). Only the main aspects of the implementation scheme are presented in this paper, more details are given in [15].

During a typical iteration of a non-linear problem, the initial state, history variables and the increment of the generalised strains are known at each integration point. The stresses must be numerically updated in order to be consistent with this generalised

strains increment. The first stage in the procedure is the division of the given generalised strain increment into a number of sub-steps by defining a pseudo time τ [2]:

$$\tau = \frac{(t - t_0)}{\Delta t} \quad 0 \leqslant \tau \leqslant 1 \tag{10}$$

where t_0 is the time at the start of the considered increment (global system) and $(t_0 + \Delta t)$ is the time at the end of this increment. Below, the main stages to update stresses and history variables are described.

A number of different procedures must be used in the constitutive law integration process. Initially, a generalised strain subincrement inside the LC is assumed (Section 4.1). After the stress integration, it must be verified whether the stress increment still remains inside the main LC yield locus and if this is not the case the yield surface contact point must be determined (Section 4.2). The integration of the strain subincrement going outside the main yield surface must distinguish between the case where only one mechanism is active (Section 4.3) or two mechanism are acting simultaneously (Section 4.4). Finally, the rare case of a purely elastic increment is considered in Section 4.5.

4.1. Integration of the generalised elasto-plastic law (irreversible mechanism associated with the coupling between the two structural levels)

In this section, the case of a stress state that remains inside the LC yield curve is examined (Case II). In this case, therefore, the generalised plasticity model applies. As explained in [7], the generalized plasticity theory offers different alternatives to model elasto-plastic behaviour. Here, it has been assumed that there is no specific elastic response related to this mechanism [7]. Therefore, to determine which one of the microstructural stress paths is active, the loading/unloading criteria given by (5)–(7) is expressed in terms of tolerances, (as required by numerical implementation) as follows:

$$\hat{\mathbf{n}}_C^T \cdot \dot{\hat{\sigma}}^e > \text{CTOL} \rightarrow \text{Microstructural compression path (MC)} \tag{11}$$

$$\hat{\mathbf{n}}_S^T \cdot \dot{\hat{\sigma}}^e > \text{CTOL} \rightarrow \text{Microstructural swelling path (MS)} \tag{12}$$

$$\left.\begin{array}{l} \hat{\mathbf{n}}_C^T \cdot \dot{\hat{\sigma}}^e < \text{CTOL} \\ \hat{n}_S^T \cdot \dot{\hat{\sigma}}^e < \text{CTOL} \end{array}\right\} \rightarrow \text{Neutral Loading (NL)} \tag{13}$$

where CTOL is a tolerance associated with the loading criteria of the coupling mechanism between structures.

The Euler's scheme with error control and sub-stepping proposed by Sloan et al. [2] to integrate conventional elasto-plastic laws has been adopted to update the stresses for the generalised plasticity model. In Sloan's algorithm the size of each sub-increment may vary through the integration process, depending on the degree of non-linearity of the constitutive relations. Considering a pseudo time sub-increment in the range $0 \leqslant \Delta\tau_n \leqslant 1$, and using the subscript $n-1$ and n to denote quantities computed at the pseudo times τ_{n-1} and $\tau_n = \tau_{n-1} + \Delta\tau_n$, the generalised strains for this sub-increment are given by

$$\Delta\boldsymbol{\varepsilon}_n = \Delta\tau_n \Delta\boldsymbol{\varepsilon} \quad \text{(a)}; \quad \Delta s = \Delta\tau_n s \quad \text{(b)}; \quad \Delta T = \Delta\tau_n T \quad \text{(c)} \tag{14}$$

With the explicit Euler method, the stress increments (9) at the end of the pseudo time step $\Delta\tau_n$ are evaluated through:

$$\Delta\boldsymbol{\sigma}_1 = \mathbf{D}_{ep|\sigma_{n-1},r_{n-1}|} \cdot \Delta\boldsymbol{\varepsilon}_n + \gamma_{s|\sigma_{n-1},s_{n-1},r_{n-1}|}\Delta s + \gamma_{T|\sigma_{n-1},T_{n-1},r_{n-1}|}\Delta T \tag{15}$$

where $\mathbf{X}_{|\sigma_{n-1},r_{n-1}|}$ means that the matrix $\mathbf{X}$ is evaluated at σ_{n-1} and r_{n-1}. The expressions of $\mathbf{D}_{ep}$, γ_s and γ_T are given in the Appendix A (Eqs. A(14), A(15) and A(16), respectively). The estimated value of stresses and internal variables are obtained from:

$$\boldsymbol{\sigma}_n = \boldsymbol{\sigma}_{n-1} + \Delta\boldsymbol{\sigma}_1 \tag{16}$$

A more accurate estimation of the stresses increment at the end of the interval $\Delta\tau_n$ can be found using the modified Euler procedure:

$$\Delta\boldsymbol{\sigma}_2 = \mathbf{D}_{ep|\sigma_n,r_n|} \cdot \Delta\boldsymbol{\varepsilon}_n + \gamma_{s|\sigma_n,s_n,r_n|}\Delta s + \gamma_{T|\sigma_n,T_n,r_n|}\Delta T \tag{17}$$

The following estimation of the stresses and internal variables can then be made using:

$$\tilde{\boldsymbol{\sigma}}_n = \boldsymbol{\sigma}_{n-1} + \frac{1}{2}(\Delta\boldsymbol{\sigma}_1 + \Delta\boldsymbol{\sigma}_2) \tag{18}$$

The relative error measure (R_n) can be obtained as [1]

$$R_n = \frac{1}{2}\frac{\|\Delta\boldsymbol{\sigma}_2 - \Delta\boldsymbol{\sigma}_1\|}{\|\tilde{\boldsymbol{\sigma}}_n\|}. \tag{19}$$

The updating of the current sub-increment is accepted if R_n is not greater than the prescribed tolerance, STOL, and it is rejected otherwise. If it is rejected, a reduction of the size of the sub-increment is made and the integration process is repeated considering the new (reduced) generalised strain sub-increment (more details are given in Section 4.6). This loop is repeated until the prescribed value of error tolerance is satisfied. When the acceptance condition is met, and before updating the stresses, it is necessary to check whether the new stress state remains inside the LC yield surface as described in Section 4.2. If the stress state still remains in the yield surface, stresses and internal variables are updated according to

$$\boldsymbol{\sigma}_n = \tilde{\boldsymbol{\sigma}}_n \quad \text{(a)}; \quad r_n = \tilde{r}_n \quad \text{(b)} \tag{20}$$

Then, the size of pseudo time sub-interval is automatically adjusted (as described in Section 4.6) and a new sub-step can be started.

4.2. Intersection with the LC yield surface

At the end of each elasto-plastic sub-increment corresponding to Case II (i.e. only the plastic mechanism associated with the interaction between structures is active, Section 4.1) or each elastic sub-increment (Section 4.5); a check is performed to verify whether the stress state still lies inside the LC yield surface. The activation of the plastic mechanism associated with macrostructural yielding occurs if

$$F_{n-1} = F_{|\sigma_{n-1},r_{n-1}|} < 0 \quad \text{and} \quad F_n = F_{|\sigma_n,r_n|} > 0 \tag{21}$$

In this case, to determine the portion of the stress increment that lies within the yield surface, it is necessary to find a scalar μ such as [1]:

$$\boldsymbol{\sigma}_{in} = \boldsymbol{\sigma}_{n-1} + \Delta\boldsymbol{\sigma}^e(\mu\Delta\boldsymbol{\varepsilon}) \quad \text{(a)}; \quad F_{in} = 0 \quad \text{(b)} \tag{22}$$

The scalar μ lies within the range $0 < \mu < 1$. value of μ equal to zero it implies a purely elasto-plastic deformation during the sub-step, whereas when it is equal to one it indicates a response inside the LC yield surface during the sub-step. In general, μ gives the portion of the generalised strains sub-increment that moves the stresses from σ_{n-1} to the intersection with the yield surface σ_{in}. The exact condition (22) (b) is replaced by $|F_{in}| < $ FTOL, were FTOL is a small positive tolerance [2]. The value of μ is obtained solving a non-linear system. The Newton–Rapshon scheme proposed by Sloan [1] has been extended for this model:

$$\begin{aligned} \boldsymbol{\sigma}_k &= \boldsymbol{\sigma}_{k-1} + \mu_k \mathbf{D}_e \Delta\boldsymbol{\varepsilon} \\ \mu_{k+1} &= \mu_k + \Delta\mu_{k+1} \\ \Delta\mu_{k+1} &= -\frac{F_k}{(\partial F/\partial\boldsymbol{\sigma})_k^T \Delta\boldsymbol{\sigma} + (\partial F/\partial s)_k \Delta s + (\partial F/\partial T)_k \Delta T} \end{aligned} \tag{23}$$

The iterative procedure is started by assuming $\sigma_0 = \sigma_{n-1}$ and a seed value for μ_1, and continues until a relative error in the norm of stresses, defined by the following Equation, is less than some specified tolerance ITOL

$$\frac{\|\boldsymbol{\sigma}_{k+1} - \boldsymbol{\sigma}_k\|}{\|\boldsymbol{\sigma}_k\|} < \text{ITOL} \tag{24}$$

Following the procedure proposed in [2], the Newton–Rapshon scheme has been combined with a bisection algorithm used when the Newton–Raphson scheme does not converge after 10 iterations in order to increase the robustness of the procedure. Once (24) is satisfied the stresses and internal variables are updated using (25); and the plastic part of the generalised strains increments $(1 - \mu)$ is integrated according to Section 0, if only the LC plastic mechanism is active, or Section 4.4, if both plastic mechanisms are active

$$\boldsymbol{\sigma}_n = \boldsymbol{\sigma}_k \quad \text{(a)}; \quad r_n = r_k \quad \text{(b)} \tag{25}$$

Sometimes, the LC yield curve can be non-convex, notably in the transition between saturated and unsaturated states [20]. In that case, especial procedures are required, involving, for instance, change of stress variables and smoothing of derivatives. A novel and efficient solution to this problem has been recently proposed [21].

4.3. Integration of the macrostructural elasto-plastic law, BBM (irreversible mechanism associated with the yielding of the macrostructure)

The case of yielding of the macrostructure alone is now considered (Case III). The procedure to integrate the elasto-plastic law is analogous to that described in Section 4.1, but now the elasto-plastic operators (A17), (A18) and (A19) (see Appendix A) are used in (15) and (17). Once the error criterion for the elasto-plastic integration is fulfilled (i.e. $R_n \leqslant \text{STOL}$, with R_n according to (19)), stresses and internal variables are updated (18). Depending on whether the sub-increment stress integration is accepted or rejected, the pseudo time is automatically adjusted for the next sub-step. Details of the sub-stepping strategy are presented in Section 4.6.

At the end of each elasto-plastic sub-step it is necessary to check whether the stress state lies on the yield surface. In this scheme it is possible that the accepted updated stresses (at the end of the sub-increment) do not satisfy the yield criterion, i.e. |Fn| > FTOL. As such departures are cumulative during the integration process, it is necessary to ensure that the stresses are corrected at the end of each sub-increment in order to satisfy the yield condition and, consequently, update accurately the stresses. This step is sometimes known as 'yield surface drift correction'. The method proposed in [22] has been adopted. The basic assumption is the consideration of a constant total strain during the correction process. In this model, it is also assumed that during the correction process, suction and temperature remain constant. This implies that an elastic strain change must be balanced by an equal and opposite change in the plastic strains.

Following [22,2], the required corrections can be obtained as

$$\delta\boldsymbol{\varepsilon}^e = [\mathbf{D}_e]^{-1}(\boldsymbol{\sigma}_c - \boldsymbol{\sigma}_n) \quad \text{(a)}; \quad \delta\boldsymbol{\varepsilon}^p = \mu_c \frac{\partial G}{\partial \boldsymbol{\sigma}} \quad \text{(b)} \tag{26}$$

Combining (26) (a) and (b) and considering the changes in the hardening parameter, the following set of equations is obtained:

$$\boldsymbol{\sigma}_c = \boldsymbol{\sigma}_n - \mu_c \mathbf{D}_e \frac{\partial G}{\partial \boldsymbol{\sigma}} \quad \text{(a)}; \quad r_c^h = r_b^h + \mu_c \delta r^h \frac{\partial G}{\partial \boldsymbol{\sigma}} \quad \text{(b)} \tag{27}$$

where μ_c is a scalar computed as

$$\mu_c = \frac{F_{|\sigma_n, r_n^h|}}{\left(\frac{\partial F}{\partial \boldsymbol{\sigma}}\right)^T \mathbf{D}_e \frac{\partial G}{\partial \boldsymbol{\sigma}} - \left(\frac{\partial F}{\partial r^h}\right)^T \delta r^h \frac{\partial G}{\partial \boldsymbol{\sigma}}} \tag{28}$$

This scheme has to be applied repeatedly until the yield condition (|F_c| < FTOL) is satisfied.

4.4. Integration of the elasto-plastic law when two plastic mechanisms are active

When two irreversible mechanisms are active simultaneously, i.e. macrostructural yielding plus one of interaction mechanisms active (Case IV), the integration process used is the same as indicated in Section 4.1, but now the elasto-plastic matrix and vectors correspond to those indicated in the Appendix A for Case IV, i.e. (A20), (A21) and (A22). If the step is accepted, stresses and internal variables are updated. If not, the sub-increment is re-started (see Section 4.6). Finally, at the end of each successful sub-increment, the correction of stresses and internal variables due to the 'yield surface drift' is performed according to a procedure similar to that described previously in Section 4.3.

4.5. Elastic stress integration

Due to the formulation of the model, purely elastic stress increments are not very common and they are limited to stress paths that move on the neutral line (Section 2.2) and inside the LC yield surface. For those cases, the stress integration scheme adopted is similar to that described in Section 4.1 but now integration involves the elastic operators (see Appendix A, Eqs. A10, A12 and A13). At the end of the sub-increment, it is checked whether the trial stress state is outside the yield surface (Section 4.2), if not, no plastic yield occurs and the stress state is updated with the trial stress state.

4.6. Sub-stepping strategy

The stepping procedure suggested by Sloan et al. [2] has been adapted for the integration of this constitutive model. As a main feature of this strategy, it can be mentioned that once the local error has been computed for a given step, the size of the next step is evaluated considering the result of this error estimation. Therefore, the size of the each sub-interval is adjusted according to the information of the previous step. This error control allows the automatic variation of the size of the interval over the course of the integration, depending on the degree of non-linearity of the model. The sub-increment strategy and the main stages of the integration can be summarized in 10 stages, as follows:

1. The integration scheme is started with the known initial state (stresses and internal variables) and the generalised strains increment.
2. An initial pseudo time step is assumed, $\Delta\tau_1$ (a value of 0.5 is typically adopted).
3. The generalized strains sub-increment is obtained from (14).
4. The integration procedure indicated in Section 4.5 is performed in the case of an elastic integration or the one indicated in Sections 4.1, 4.3 or 4.4 in the case of an elasto-plastic integration.
5. After a successful elastic sub-increment (Case I), it is necessary to check if the updated stress state remains inside the yield surface (Section 4.2).
   - If the sub-increment is purely elastic the stresses and history variables are updated according to Eq. (20). Then the pseudo time is checked according to stage 10.
   - If the sub-increment stresses cross the LC yield surface, stresses and internal variables are updated with the elastic portion (25). The plastic part of the sub-increment is integrated according to Sections 4.2, 4.3 or 4.4 depending on which elasto-plastic mechanism(s) is/(are) active.

6. After a successful elasto-plastic sub-increment and before checking the pseudo time, it is necessary to verify the following points:
   - If the sub-increment corresponds to a Case II (i.e. only the interaction mechanism is active), it is necessary to check if the updated stress remains inside the LC yield surface (Section 4.2):
     ○ If the stress remains inside the LC curve, stresses and history variables are updated according to Section 4.1. Then the pseudo time is checked according to stage 10.
     ○ If the stress sub-increment crosses the LC yield surface, stresses and internal variables are updated with the elastic-plastic portion corresponding to Case II (Section 4.1). The other portion of the elasto-plastic sub-increment, which corresponds to Case IV (i.e. two elato-plastic mechanisms active), is integrated according to Section 4.4.
   - If the sub-increment corresponds to a Case II or IV, it is necessary to correct for the drift of the yield surface according to Section 4.3. Then the pseudo time is checked according to stage 10.
7. The relative error measure (R_n) is computed (19) and q is evaluated as

$$q = 0.95\sqrt{STOL/R_n}, \quad \text{with the constraint}: 0.2 \leqslant q \leqslant 1.2 \tag{29}$$

8. Regardless of whether the sub-increment is accepted or not, the next pseudo time step is automatically adjusted as

$$\Delta\tau_{n+1} = q\Delta\tau_n \tag{30}$$

9. After a refused sub-increment (elastic or elasto-plastic), a new sub-increment is re-started with a smaller step-size (30) and with reduced generalized strains sub-increments according to (14). This loop is repeated until a successful sub-increment size is obtained. Here, an additional control is imposed in order to avoid an excessive number of iterations. The user can establish a maximum number of iterations to reach a successful integration. On reaching that number, the integration process is aborted and a reduction of the time increment is imposed over the global system. This strategy yields good results, especially when complex highly non-linear problems are modelled.
10. The sub-stepping integration continues until the entire increment of the generalized strains is applied, verified through:

$$\sum \Delta\tau = \tau = 1 \tag{31}$$

Note that the generalized plasticity model is integrated with the same degree of accuracy and efficiency that the conventional BBM elasto-plastic law. From the algorithm point of view, the main difference is that the 'yield surface drift correction' is omitted in a generalized plasticity model, as no yield surface is explicitly defined.

5. Application case

The mechanical model has been widely validated at integration point level in a number of applications [6,7]. In those works, the capabilities of the model to describe and predict the behaviour of expansive soils under complex stress paths have been established. In this paper, the aim is to explore the performance of the model and its implementation in FE when it is applied to the solution of a coupled THM boundary value problem. The case selected involves the THM behaviour of the FEBEX mock-up test, a large-scale heating experiment [23].

The layout of the mock-up test is depicted in Fig. 3. Two electrical heaters (simulating canisters containing heat-emitting waste) were placed in the centre of a steel cylinder 6 m long and with an inner diameter of 1.62 m. The space between the heaters and the steel cylinder was filled with a 0.64 m-thick engineered barrier made up of blocks of compacted FEBEX bentonite. The barrier is hydrated uniformly from all around the cylinder with an applied water pressure of about 0.5 MPa. Simultaneously, the barrier was heated maintaining a constant temperature of 100 °C at the contact between heaters and bentonite. The evolution of the main THM variables of the test (temperature, heater power, water intake, relative humidity and stresses) is recorded by several sensors placed inside the barrier in different sections symmetrically placed respect to the centre of the barrier (Fig. 3 shows the sections analyzed in this work).

The test has been modelled taking advantage of the basic axial symmetry of the problem and of the relatively long size of the heaters in order to adopt a radial 1-D discretization. All the analyses have been carried out using the computer program CODE_B-RIGHT [8]. The geometry of the problem as well as the initial and boundary conditions have been based on [23]. An initial temperature of 20 °C has been prescribed together with and initial hydrostatic net stress of 0.11 MPa (approximately equal to the weight of the bentonite in the mid diameter of the buffer). Finally, the initial values of relative humidity (RH) recorded in the test have been
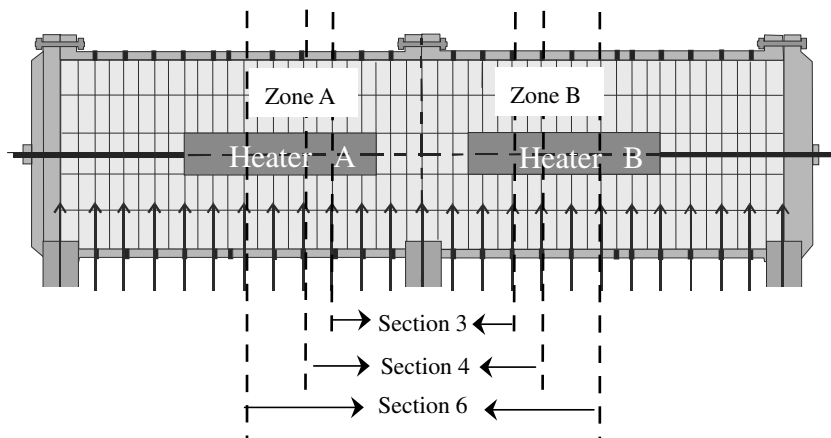

Fig. 3. Layout of the mock-up test.

used to estimate and prescribe the initial suction. Regarding boundary conditions, a water pressure of 0.55 MPa has been applied on the external part of the bentonite barrier and a stress free condition has been prescribed on the outer boundary of the steel cylinder. Finally, the thermal boundary conditions at a radius equal to 0.15 m (radial coordinate of the heater elements) are as follows: a staggered increase of heater power has been applied until a temperature of 100 °C is reached at the contact between heater and bentonite (at 15.6 days), afterwards a constant temperature of 100 °C has been maintained at this contact point. On the external boundary of the steel cylinder, a thermal radiation condition has been applied [24].

A key feature of this test is that due to simultaneous heating and hydration a series of coupled THM phenomena take place in the clay barrier inducing cycles of wetting and drying in different zones of the buffer. For illustration purposes, Fig. 4 presents the evolution of the RH at two points of a typical section of the barrier. The behaviour of the part of the buffer near heater is very characteristic (sensors at a distance from the axis, $r = 0.22$ m). There is an initial wetting due to the condensation of the vapour coming from the inner barrier regions (values higher than 60% have been recorded at this stage). However, drying takes place eventually due to the combined effect of temperature increase and reduced vapour arrival. Finally, a gentle hydration is observed due to the inflow of water coming from the outer barrier regions. On the other hand the external part of the barrier (sensors at a distance from the axis, $r = 0.70$ m) is subjected to continuous hydration from the beginning of the test.

A complete study of the evolution of the THM variables of the mock-up is presented elsewhere [15,24], herein the attention is focused mainly on the evolution of the basic variables of the mechanical model and on the main mechanisms that control the mechanical response of the clay during the experiment. The core of the formulation used in this analysis is the double structure model summarized in the previous sections and presented in detail in [15]. A wide ranging experimental campaign has been carried to study the behaviour of FEBEX bentonite, that has allowed the determination of the main parameters of the double structure model [6,24]. Table 2 summarizes the model parameters used in the analysis (more details can be found in [24]). A procedure to determine the main parameters of this model has been presented in [6].
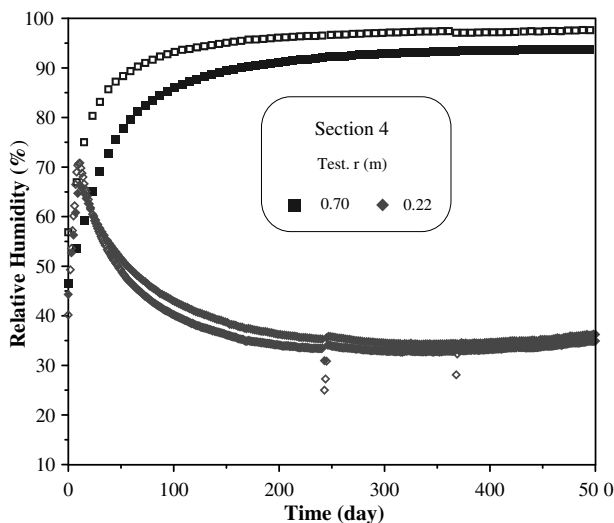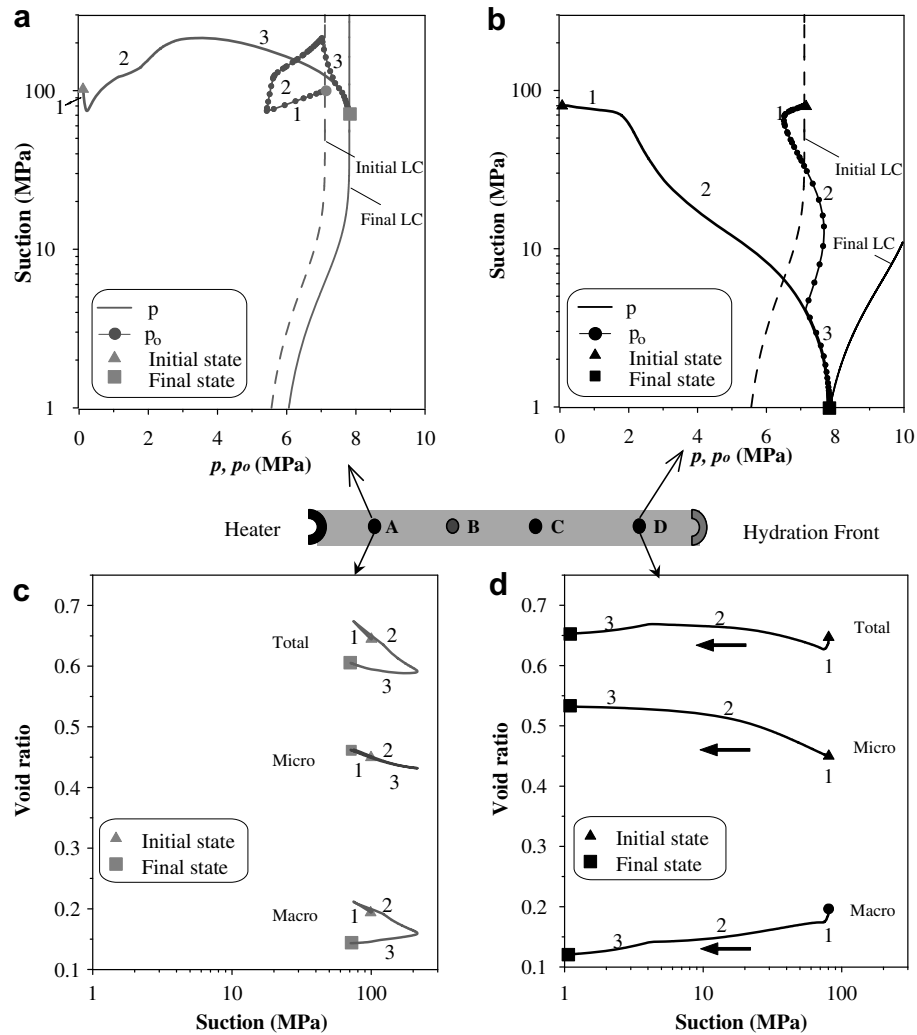
Table 2
Parameters used to define the elasto-plastic constitutive law

Parameters defining the Barcelona Basic Model for macrostructural behaviour

κ	κ_s	$\lambda_{(0)}$	r	p_c (MPa)	ζ (MPa^{-1})	p_o^* (MPa)	α_0 (°C^{-1})
0.005	0.001	0.080	0.90	0.50	0.20	5.5	1.0 e^{-5}

Parameters defining the law for microstructural behaviour

α_m (MPa^{-1})	β_m (MPa^{-1})	χ
2.1e^{-02}	2.3e^{-03}	1

Interactions functions

$f_C = 1 + 0.9 \tan h(20(p_r/p_0) - 0.25)$; $f_S = 0.8 - 1.1 \tan h(20(p_r/p_0) - 0.25)$

e_{macro}	e_{micro}
0.20	0.45

Tolerances

| STOL	CTOL	FTOL	ITOL
1.0E-05	1.0E-05	1.0E-08	1.0E-08

The algorithm described must therefore deal with a wide variety of situations. In order to illustrate the complexity of the couplings between the various THM phenomena and of the interaction between the two structural levels, the behaviour of the two selected points with the same radial coordinates, as in Fig. 4, is now described in some detail using Figs. 5 and 6. Fig. 5a and b present the generalized-stress path on the p–s plane, together with the evolution of p_0 (apparent preconsolidation stress for the current value of suction) in terms of suction; whereas Fig. 5c and d present the changes of void ratio (macro, micro and total) in terms of suction, as computed by the model. Finally, Fig. 6a and b depict the evolution of the values of the interaction functions movement in the various stages of the analysis.

Considering first the position close to the heater (point A, $r = 0.22$ m), three main stages can be distinguished after the 'start of heating and hydration' (indicated as 'initial state' in Fig. 5): (1) wetting due to water vapour condensation, (2) strong drying induced by the heater, and (3) final hydration. From the beginning the test undergoes wetting (from the external part inwards), which induce clay swelling and, due to the confined conditions of the test; a global increment of the net stress is computed. Stage '1' (Fig. 5a and c and Fig. 6a is characterized by a suction reduction (due to the condensation of the water vapour) at a very low value of p. This implies swelling at both pore levels. The microstructure swells due to a reduction of the generalized microstructural stress (mainly due to suction reduction); and the macrostructure expands by the combined effects of suction reduction and also due to the active interaction mechanism (MS path) that induces plastic macrostructural swelling strains, due to the positive values of the interaction function f_s (4). This mechanism implies a softening of the macrostructure with a reduction of p_0^*. Stage '2' is characterized by strong drying in zones close to the heater. During this stage, hydration progresses in the external zones of the barrier and induces a steady increase of the stress level. Those two facts cause a rise of the generalized microstructural stress and, consequently, a contraction of the microstructure (MC path). The coupling mechanism between micro and macro structure induces positive (contractive) plastic macrostructural strains due to the positive values of the interaction function f_c. The macrostructure also contracts due to the combined effect of p and suction increments. So, this stage implies a macrostructural hardening. Finally, stage '3' is related to the final hydration stage of this zone, controlled by a gradual reduction of suctions and a significant increase of p. During the MS path the interaction function f_s has negative values, which implies a hardening of the macrostructure associated to a wetting process under high pressure [4]. At a suction close to 110 MPa, the stress path reaches the LC curve and drags it along until the end of the analysis.

Fig. 4. Evolution of relative humidity in Section 4, mock-up test. Note that for each radial coordinate, the observations of two sensors are plotted, corresponding to the two symmetric halves of the experiment.

Fig. 5. (a) and (b) Generalized-stress path on the p–s and $p_0 - s$ plane and (c) and (d) void ratio (total, macro and micro) vs. suction for 2 characteristics points of the barrier: A (r = 0.22 m) and D (r = 0.70 m).
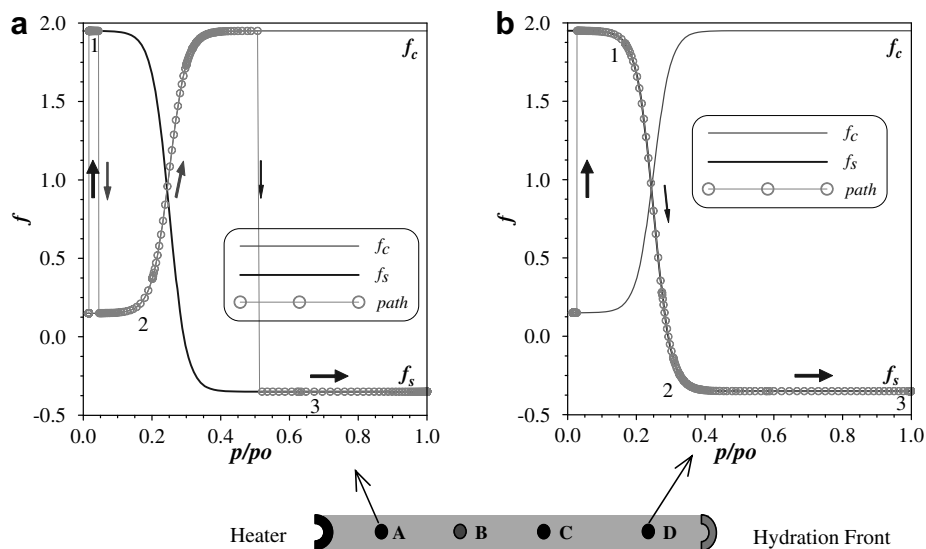
Fig. 6. (a) and (b) Evolution of the values of the interaction functions movement in the various stages of the analysis for 2 characteristics points of the barrier: A (r = 0.22 m) and D (r = 0.70 m).

Close to the hydration boundary (point *D*, *r* = 0.70 m), a quite different behaviour is observed (Fig. 5b and d and Fig. 6b). Three main stages have been identified here as well. Stage '1' is characterized by a slight suction reduction (the hydration front has not reach this zone yet) and a noticeable stress increment given by the progressive hydration of the external part of the barrier. During this stage the main compression corresponds to the closing of the macropores due to the dominant effect of the stress increment. The microstructure expands, due to reduction of the microstructural effective stress (3a). Due to the positive values of the interaction function fs during the MS path a macrostructural softening (reduction of p_0^*) is predicted. Stage '2' maintains this tendency to suction reduction and stress increase, but now the suction reduction is more noticeable (the hydration front is reaching this zone). This implies a large microstructural swelling due to the strong reduction of microstructural effective stress (3a). This microstructural expansion, under confined conditions, tends to increase the stress level and compresses even more the macropores. Finally, stage '3' starts when the stress path reaches the LC curve. After that, the stress path drags the LC curve with it and both move together. The shape of the stress path in this last stage is mainly controlled by the LC curve. During this stage the macropores reduction takes place under small changes of stresses, i.e. a kind of macrostructural collapse occurs in this zone of the barrier at advanced phases of hydration.

Comparing Fig 5a and b it can be observed that the generalized stress paths are quite different. In addition, there is an important increment of the elastic domain in zones corresponding to point 'D' ('Final LC' in Fig. 5b). The hardening of the material is due to the reduction of macropores induced, mainly, by the microstructural expansion during hydration under confined conditions. The coupling between micro and macro structure is the crucial mechanism to model this behaviour. The tendency of expansive clays to a macropore reduction under confined conditions during hydration has been experimentally observed [25]. The use of this advanced model that allows the inclusion of the soil fabric effects in the analysis it is a crucial aspect to describe the complex clay behaviour observed in the mock-up test [24].

The performance of the model was very satisfactory. For illustration, two additional figures showing comparisons between experiment and model results are presented below. Fig. 7a shows the evolution of radial stress for two typical sections (Sections 3A& B and 6A& B, see Fig. 3). As it can be observed, the model reproduces quite well the quick increase of radial stress at the beginning of the hydration and also the maximum value of radial

stress observed in the test. Fig. 7b also shows that the model is able to capture reasonably well the evolution of the RH during the first complex stages of the test. More details of the mock-up test modelling can be found in [24]. Complex THM behaviour has thus been successfully tracked using a generalized plasticity constitutive law for a double structure material and the implementation algorithm described in the paper.

To check the accuracy and efficiency of the proposed algorithm, the same analysis has been performed using decreasing values of the stress tolerances STOL and CTOL that are assumed equal. The rest of model parameters and tolerances have maintained unchanged (Table 2). Table 3 presents the following variables for the different computations carried out: 'CPU time', 'Radial stress, 'Total sub-steps' and 'Stress error'. The numerical analyses have been performed using A Sillicon Graphics Origin 300 (8 processors MIPS R14000 at 600 MHz, 6 GB RAM memory) computer. The CPU time recorded is not for the integration algorithm alone but for the entire computation. The 'Stress error' (σ_{error}) has been evaluated according to [2]:

$$\sigma_{error} = \frac{\left\{ \sum_{i=1}^{m} \left[(\sigma_{ref} - \sigma)^T (\sigma_{ref} - \sigma) \right]_i \right\}^{1/2}}{\left\{ \sum_{i=1}^{m} [(\sigma_{ref})^T (\sigma_{ref})]_i \right\}^{1/2}} \tag{32}$$

where the subscript *i* refers to each integration point, *m* is the total number of integration points in the mesh, σ are the stresses computed at the end of the last load increment and σ_{ref} are the 'reference stresses'. The results obtained with a STOL = CTOL = 10^{-7} have been adopted as σ_{ref}. The 'radial stress' and 'total sub-steps' correspond to a representative integration point in an element near the hydration boundary (*r* = 0.80 m).

It can be observed that there are not significant differences in the CPU times required when the imposed tolerance (STOL) is higher than 10^{-4}; while the CPU times required for tolerances below this value increase dramatically. This implies that when low values of tolerances are prescribed, the total CPU required is mainly spent in the stress integration process, as it can be observed in the number of total steps required. As the tolerances are reduced an asymptotic tendency for a slight radial stress reduction is computed. As it should be expected, the accuracy of the algorithm increases as the tolerances are reduced but quite small errors are still obtained with the larger stress tolerances, with the resulting savings in CPU times.
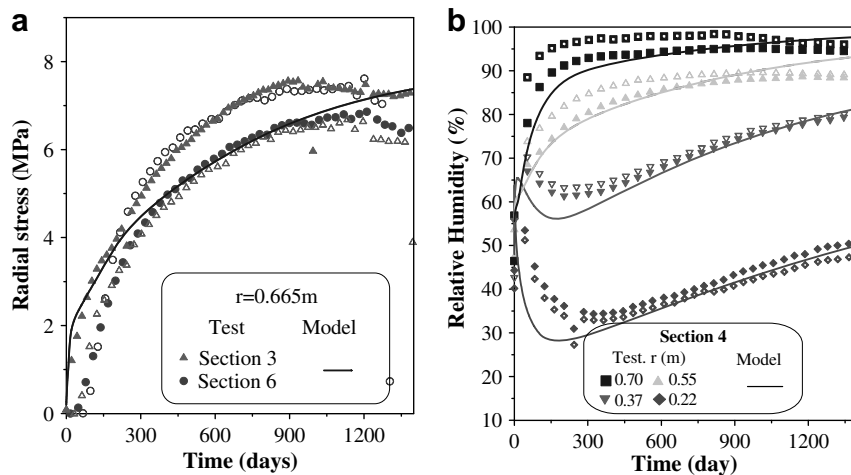

Fig. 7. (a) Evolution of stresses in two different sections of the mock-up test (Sections 3A & B and 6A & B) and evolution of relative humidity in different radii of Section 4.

Table 3
Effect of stress tolerances on algorithm performance and stress error

STOL = CTOL	CPU time (s)	Radial stress (MPa)	Total sub steps	Stress error σ_{error}
1.0E-01	1614	7.91221	13416	83.9E-04
1.0E-02	1614	7.91221	13416	83.9E-04
1.0E-03	1616	7.91220	13450	83.2E-04
1.0E-04	1620	7.91216	13452	81.5E-04
1.0E-05	1787	7.90938	15999	4.87E-04
1.0E-06	2437	7.90680	25503	1.57E-04
1.0E-07	4518	7.90549	52100	0.00E+00

6. Conclusions and final remarks

In this paper an algorithm to implement a double structure model for expansive clays in a finite element code has been presented. The algorithm is based on Sloan's scheme [1,2] and has been specifically adapted to the characteristics of this model. The algorithm has been extended to update stresses and internal variables in terms of the increment in generalized strains that include strains, suction and temperature. Another extension of the scheme is related to the handling of more than one irreversible mechanism. The same modified scheme has been used to integrate the two elasto-plastic laws (one based on classical plasticity and one based on generalized plasticity) and the highly non-linear elastic law. This ensures the integration of the different parts of the model with the same degree of accuracy and efficiency. The performance of the model in the application case presented herein has been very satisfactory with a good level of efficiency and robustness. A good reproduction of a complex THM case has been achieved and, in addition, a physical interpretation of the observed behaviour within the context of double structure media has also been obtained. Most of the main features of the behaviour are correctly reproduced by the model allowing a more detailed examination of the role that the different variables play in relation to the overall behaviour of the clay barrier submitted to heating and hydration under confined conditions. A sensitivity analysis has illustrated the dependency of the efficiency and accuracy of the algorithm with the values of stress tolerances adopted.

Acknowledgements

Appendix A. Mechanical model

The BBM yield surface (F_{LC}) is given by (3) and the plastic potential (G) is expressed as

$$G = \alpha 3J^2 - \left[\frac{g(\theta)}{g(-30^0)}\right]^2 M^2 (p + p_s)(p_0 - p) = 0 \tag{A1}$$

where α is determined according to [12]. The dependence of the tensile strength on suction and temperature is given by

$$p_s = kse^{-\rho\Delta T} \tag{A2}$$

where k and ρ are model parameters. The dependence of p_0 on suction and temperature is given by

$$p_0 = p_c \left(\frac{p_{0T}^*}{p_c}\right)^{\frac{\lambda_{(0)}-\kappa}{\lambda_{(s)}-\kappa}} \quad \text{(a)};$$

$$p_{0T}^* = p_0^* + 2(\alpha_1\Delta T + \alpha_3\Delta T|\Delta T|) \quad \text{(b)} \tag{A3}$$

where p_c is a reference stress, α_1 and α_3 are models parameters. $\lambda_{(s)}$ is the compressibility parameter for changes in net mean stress for virgin states of the soil. This parameter depends on suction according to

$$\lambda_{(s)} = \lambda_{(0)}[r + (1 - r)\exp(-\zeta s)] \tag{A4}$$

where r is a parameter which defines the minimum soil compressibility (at infinite suction) and ζ is a parameter which controls the rate of decrease of soil compressibility with suction. The macrostructural bulk modulus (K_M) for changes in mean stress is evaluated with the following law:

$$K_M = \frac{(1 + e_M)}{\kappa}p \tag{A5}$$

The microstructural bulk modulus (K_1) is evaluated as follows:

$$K_m = \frac{e^{-\alpha_m\hat{p}}}{\beta_m} \tag{A6}$$

where α_m and β_m are model parameters. The shear modulus G_t is obtained from a linear elastic model as follows:

$$G_t = \frac{3(1 - 2\mu)K}{2(1 + \mu)} \tag{A7}$$

where μ is the Poisson's coefficient. The macrostructural bulk modulus for changes in suction is computed considering the following law:

$$K_s = \frac{(1 + e_M)(s + p_{atm})}{\kappa_s} \tag{A8}$$

where κ_s is the macrostructural elastic stiffness parameter for changes in suction. The macrostructural bulk modulus for changes in suction is computed considering the following law:

$$K_T = \frac{1}{(\alpha_0 + \alpha_2\Delta T)} \tag{A9}$$

where α_0 and α_2 are parameters related to the elastic thermal strain.

Elastic and elasto-plastic relationships.

Firstly, the elastic tensors related to Eq. (8) are presented. These tensors correspond to the Case identified as 'I' (Elastic sub-increment) in Section 4. The elastic matrix is evaluated as follows:

$$\mathbf{D}_e = \begin{bmatrix} K + \frac{4}{3}G_t & K - \frac{2}{3}G_t & K - \frac{2}{3}G_t & 0 & 0 & 0 \\ & K + \frac{4}{3}G_t & K - \frac{2}{3}G_t & 0 & 0 & 0 \\ & & K + \frac{4}{3}G_t & 0 & 0 & 0 \\ & & & G_t & 0 & 0 \\ \text{symm} & & & & G_t & 0 \\ & & & & & G_t \end{bmatrix} \tag{A10}$$

where K is the global bulk that may be computed considering the elastic contribution of the two pores structures, the global stiffness is defined as

$$K = \left(\frac{1}{K_M} + \frac{1}{K_m}\right)^{-1} \tag{A11}$$

$$\alpha_s = \left(\frac{1}{K_s} + \frac{\chi}{K_m}\right)\mathbf{D}_e \cdot \mathbf{m} \tag{A12}$$

$$\alpha_T = \frac{1}{K_T}\mathbf{D}_e \cdot \mathbf{m} \tag{A13}$$

More details can be found in [7]. The elasto-plastic tensors related to (9) correspond to three different possibilities (Case II, III and IV) indicated in Section 4, which introduced as follows:

- Case II: when only the plastic mechanism associated with the coupling between structures is active:

$$\mathbf{D}_{ep} = \mathbf{D}_e \cdot \left[\mathbf{I} - \frac{1}{\overline{H}_\beta} \mathbf{m}_\beta \cdot \mathbf{n}_\beta^T \cdot \mathbf{D}_e \right] \tag{A14}$$

$$\gamma_s = (\alpha_s + \beta_s) - \frac{1}{\overline{H}_\beta} \mathbf{D}_e \cdot \mathbf{m}_\beta \mathbf{n}_\beta^T \cdot (\alpha_s + \beta_s) \tag{A15}$$

$$\gamma_T = \alpha_T - \frac{1}{\overline{H}_\beta} \mathbf{D}_e \cdot \mathbf{m}_\beta \mathbf{n}_\beta^T \cdot \alpha_T \tag{A16}$$

- Case III: when only the plastic mechanism associated with the yielding of the macrostructure is active:

$$\mathbf{D}_{ep} = \mathbf{D}_e \cdot \left[\mathbf{I} - \frac{1}{\overline{H}_{LC}} \mathbf{m}_{LC} \cdot \mathbf{n}_{LC}^T \cdot \mathbf{D}_e \right] \tag{A17}$$

$$\gamma_s = \alpha_s - \frac{1}{\overline{H}_{LC}} \mathbf{D}_e \cdot \mathbf{m}_{LC} (l + \mathbf{n}_{LC}^T \cdot \alpha_s) \tag{A18}$$

$$\gamma_T = \alpha_T - \frac{1}{\overline{H}_{LC}} \mathbf{D}_e \cdot \mathbf{m}_{LC} (d + \mathbf{n}_{LC}^T \cdot \alpha_T) \tag{A19}$$

- Case IV: when two plastic mechanisms are active:

$$\mathbf{D}_{ep}$$
$$= \mathbf{D}_e \cdot \left[\mathbf{I} - \frac{1}{|\overline{\mathbf{H}}|} \left(\overline{H}_\beta \mathbf{m}_{LC} \cdot \mathbf{n}_{LC}^T - \bar{h}_\beta \mathbf{m}_{LC} \cdot \mathbf{n}_\beta^T + \overline{H}_{LC} \mathbf{m}_\beta \cdot \mathbf{n}_\beta^T - \bar{h}_{LC} \mathbf{m}_\beta \cdot \mathbf{n}_{LC}^T \right) \cdot \mathbf{D}_e \right] \tag{A20}$$

$$\gamma_s = \alpha_s + \beta_s - \frac{1}{|\overline{\mathbf{H}}|} \mathbf{D}_e \cdot \{ \overline{H}_\beta \mathbf{m}_{LC} [l + l_\beta + \mathbf{n}_{LC}^T \cdot (\alpha_s + \beta_s)]$$
$$- \bar{h}_\beta \mathbf{m}_{LC} \mathbf{n}_\beta^T \cdot (\alpha_s + \beta_s) + \overline{H}_{LC} \mathbf{m}_\beta \mathbf{n}_\beta^T \cdot (\alpha_s + \beta_s)$$
$$- \bar{h}_{LC} \mathbf{m}_\beta [l + l_\beta + \mathbf{n}_{LC}^T \cdot (\alpha_s + \beta_s)] \} \tag{A21}$$

$$\gamma_T = \alpha_T - \frac{1}{|\overline{\mathbf{H}}|} \mathbf{D}_e$$
$$\cdot \left[\overline{H}_\beta \mathbf{m}_{LC} (d + \mathbf{n}_{LC}^T \cdot \alpha_T) - \bar{h}_\beta \mathbf{m}_{LC} \mathbf{n}_\beta^T \cdot \alpha_T + \overline{H}_{LC} \mathbf{m}_\beta \mathbf{n}_\beta^T \cdot \alpha_T \right.$$
$$\left. - \bar{h}_{LC} \mathbf{m}_\beta (d + \mathbf{n}_{LC}^T \cdot \alpha_T) \right] \tag{A22}$$

where the definition of these variables are as follows:

$$l_{LC} = \frac{\partial F_{LC}}{\partial s} \tag{A23}$$

$$d = \frac{\partial F_{LC}}{\partial T} \tag{A24}$$

$$\overline{H} = \frac{\partial F_{LC}}{\partial p_0} \frac{\partial p_0}{\partial p_0^*} \frac{\partial p_0^*}{\partial \varepsilon_v^p} \tag{A25}$$

$$\dot{\varepsilon}_{vLC}^p = \dot{\lambda}_{LC} \mathbf{m}^T \cdot \mathbf{m}_{LC} \tag{A26}$$

$$\dot{\varepsilon}_{v\beta}^p = \dot{\lambda}_\beta \mathbf{m}^T \cdot \mathbf{m}_\beta \tag{A27}$$

$$\overline{H}_{LC} = H_{LC} + H_{LC}^c = H_{LC} + \mathbf{n}_{LC}^T \cdot \mathbf{D}_e \cdot \mathbf{m}_{LC} \tag{A28}$$

$$\bar{h}_\beta = h_\beta + h_\beta^c = h_\beta + \mathbf{n}_{LC}^T \cdot \mathbf{D}_e \cdot \mathbf{m}_\beta \tag{A29}$$

$$\dot{e}_{LC} = \mathbf{n}_{LC}^T \cdot \mathbf{D}_e \cdot \dot{\varepsilon} \tag{A30}$$

$$\dot{s}_{LC} = [l_{LC} + l_\beta + \mathbf{n}_{LC}^T \cdot (\alpha_s + \beta_s)] \dot{s} \tag{A31}$$

$$\dot{t}_{LC} = (d + \mathbf{n}_{LC}^T \cdot \alpha_T) \dot{T} \tag{A32}$$

$$\beta_s = -\frac{1}{H_\beta} \omega_\beta \chi \mathbf{D}_e \cdot \mathbf{m}_\beta \tag{A33}$$

$$H_{LC} = -\overline{H} \mathbf{m}^T \cdot \mathbf{m}_{LC} \tag{A34}$$

$$h_\beta = -\overline{H} \mathbf{m}^T \cdot \mathbf{m}_\beta \tag{A35}$$

$$l_\beta = -\frac{1}{H_\beta} h_\beta \omega_\beta \chi \tag{A36}$$

$$\bar{h}_{LC} = h_{LC}^c = \mathbf{n}_\beta^T \cdot \mathbf{D}_e \cdot \mathbf{m}_{LC} \tag{A37}$$

$$\overline{H}_\beta = H_\beta + H_\beta^c = H_\beta + \mathbf{n}_\beta^T \cdot \mathbf{D}_e \cdot \mathbf{m}_\beta \tag{A38}$$

$$\dot{e}_\beta = \mathbf{n}_\beta^T \cdot \mathbf{D}_e \cdot \dot{\varepsilon} \tag{A39}$$

$$\dot{s}_\beta = \mathbf{n}_\beta^T \cdot (\alpha_s + \beta_s) \dot{s} \tag{A41}$$

$$\dot{t}_\beta = \mathbf{n}_\beta^T \cdot \alpha_T \dot{T} \tag{A42}$$

Stress invariants

$$p = \left(\frac{1}{3}\right)(\sigma_x + \sigma_y + \sigma_z) \tag{A43}$$

$$J^2 = 1/2 \, \text{trace} \, (s^2) \tag{A44}$$

$$\theta = -\frac{1}{3} \sin^{-1}(1.5\sqrt{3} \, \det s/J^3) \tag{A45}$$

$$s = \sigma - p\mathbf{I} \tag{A46}$$

References

[1] Sloan S. Sub-stepping schemes for the numerical integration of elasto-plastic stress–strain relations. Int J Numer Meth Eng 1987;24:893–911.

[2] Sloan S, Abbo A, Sheng D. Refined explicit integration of elastoplastic models with automatic error control. Eng Comput 2001;18(1/2):121–54.

[3] Gens A, Alonso EE. A framework for the behaviour of unsaturated expansive clays. Canad Geotech J 1992;29:1013–32.

[4] Alonso E, Vaunat J, Gens A. Modelling the mechanical behaviour of expansive clays. Eng Geology 1999;54:173–83.

[5] Alonso E. Modelling expansive soil behaviour. In: Proceeding of 2nd international conference on unsaturated soils, vol. 1, Beijing, China; 1998. p. 37–70.

[6] Lloret A, Villar MV, Sánchez M, Gens A, Pintado X, Alonso EE. Mechanical behaviour of heavily compacted bentonite under high suction changes. Géotechnique 2003;53(1):27–40.

[7] Sánchez M, Gens A, Guimarães L, Olivella S. A double structure generalized plasticity model for expansive materials. Int J Numer Anal Meth Geomech 2005;29:751–87.

[8] Olivella S, Gens A, Carrera J, Alonso EE. Numerical formulation for a simulator (CODE-BRIGHT) for the coupled analysis of saline media. Eng Comput 1996;13(7):87–112.

[9] Pastor M, Zienkiewicz O, Chan A. Generalized plasticity and the modelling of soil behaviour. Int J Numer Anal Meth Geomech 1990;14:151–90.

[10] Argyris JH, Faust G, Szimmat J, Warnke EP, Willam KJ. Recent developments in the finite element analysis of prestressed concrete reactor vessels. Nucl Eng Design 1974;28:42–75.

[11] Sheng D, Sloan SW, Yu HS. Aspects of finite element implementation of critical state models. Comput Mech 2000;26:185–96.

[12] Alonso E, Gens A, Josa A. A constitutive model for partially saturated soils. Géotechnique 1990;40(3):405–30.

[13] Eekelen Van. HAM Isotropic yield surfaces in three dimensions for use in soil mechanics. Int J Num Anal Meth Geomech 1980;4:89–101.

[14] Gens A. Constitutive laws. Modern issues in non-saturated soils. Springer; 1995. p. 129–58.

[15] Sánchez M. Thermo-Hydro-Mechanical coupled analyses in low permeability media. PhD thesis, Universitat Politècnica de Catalunya, Spain; 2004.

[16] Rizzi E, Giulio M, Willam K. On failure indicators in multi-dissipative materials. Int J Sol Struct 1996;33(20–22):3124–87.

[17] Erratum: Eng Comput, 19(5/6); 2002. p. 594–594.

[18] Potts D, Zdravković L. Finite element analysis in geotechnical engineering. Theory. Bath: Thomas Telford; 1999.

[19] Sheng D, Sloan S, Gens A, Swith W. Finite element formulation and algorithms for unsaturated soils. Part I: Theory. Int J Numer Anal Meth Geomech 2003;27:745–65.

[20] Sheng D. Non convexity of the Barcelona Basic Model – comment on S.J. Wheeler, D. Gallipoli and M. Karstunen (2002;26:1561–1571). Int J Num Anal Methods in Geomech 2003;27:879–81.

[21] Sheng DC, Pedroso D, Abbo AJ. In: Proceeding of 1st European conference on unsaturated soils, Durham, UK; 2008. p. 705–11.

[22] Potts D, Gens A. A critical assessment of methods of correcting for drift from the yield surface in elastoplastic finite element analysis. Int J Num Anal Meth Geomech 1985;9:149–59.

[23] Martin PL, Barcala JM. Large scale buffer material test: mock-up experiment at CIEMAT. Eng Geology 2005;81(3):298–316.

[24] Sánchez M, Gens A. FEBEX II final report on THM modelling. Barcelona: ENRESA-70-UPC-L-5-015; 2005.

[25] Lloret A, Villar MV, Romero E. Final Report on THM laboratory tests. Madrid: ENRESA-CIEMAT/DIAE/54520/3/04; 2004.